Facies (2010) 56:231–248
DOI 10.1007/s10347-009-0197-1

ORIGINAL ARTICLE

Sea-level changes as controlling factor of early diagenesis: the reefal limestones of Adnet (Late Triassic, Northern Calcareous Alps, Austria)

Carsten Reinhold · Bernd Kaufmann

Received: 24 April 2009 / Accepted: 14 August 2009 / Published online: 10 September 2009

Abstract The uppermost Rhaetian Adnet reef is part of the Dachstein carbonate platform and is situated at the transition to the intrashelf Kössen Basin. Its diagenetic evolution is investigated focusing on dissolution cavities in the Tropfbruch quarry of Adnet (near Salzburg) stratigraphically situated immediately below the Triassic–Jurassic boundary. Sea-level changes due to global eustatic trends and regional tectonics are assumed to be the controlling factors in the development of a manifold diagenetic sequence characterized by phases of meteoric dissolution, marine and burial cementation, and internal sedimentation. Despite small-scale variations of the sequence, a superordinate pattern of diagenetic phases could be elaborated. Small-scale eustatic sea-level falls subordinate to a global regression trend caused subaerial exposures of the Adnet reef in the latest Rhaetian to earliest Hettangian. The result was karstification and meteoric dissolution of aragonitic coral skeletons (*Retiophyllia*) leading to the formation of biomoldic porosity. Coral septa which escaped dissolution were transformed into neomorphic calcite spar under meteoric–phreatic conditions. A first generation of dog-tooth cements precipitated sporadically on the altered coral skeletons. Eustatic sea-level rise in Early to Mid-Hettangian times caused a renewed flooding of the pore space of the Adnet reef by marine water and the influx of a first generation of internal sediments (IS I), derived from the karstified host rock of the Upper Rhaetian reef limestone. These internal sediments are overgrown by radiaxial-fibrous calcites (RFCs) whose oxygen-isotopic signature ($\delta^{18}O = -1.3$ (± 0.7)‰) indicates precipitation in deeper (colder) water (18–21°C) due to a first phase of drowning. An intermediate phase of eustatic sea-level lowstand in the Late Hettangian is expressed by dissolution and corrosion of RFCs. Rapid drowning of the Dachstein carbonate platform due to eustatic sea-level rise and tectonic movements took place in the Early Sinemurian and a second generation of internal sediments (IS II) derived from the Lower Sinemurian Adnet Formation is washed into the dissolution cavities. Where IS II is absent, RFCs are overgrown by a second generation of dog-tooth cements with a bright-luminescent outer rim indicating the transition to negative redox conditions in the pore water during shallow burial. Burial diagenesis is represented by blocky calcite cements which occlude the remaining pore space. Depleted oxygen-isotope values and significant Fe contents indicate precipitation under reducing redox conditions and elevated temperatures of 30–50°C at burial depths of 420–870 m. Locally, replacive saddle dolomite is the latest diagenetic phase in the Adnet reef indicating crystallization under hydrothermal influences related to compressional subduction regimes of the Penninic Ocean.

Keywords Adnet reef · Austria · Carbonate diagenesis · Late Triassic · Sea-level changes

C. Reinhold
E.ON Ruhrgas E&P GmbH, Huttropstrasse 60,
45138 Essen, Germany
e-mail: Carsten.Reinhold@eon-ruhrgas-ep.com

B. Kaufmann (✉)
Österreichische Akademie der Wissenschaften,
Kommission für die paläontologische und stratigraphische
Erforschung Österreichs (KPSOE), c/o Institut für
Erdwissenschaften, Karl-Franzens-Universität Graz,
Heinrichstrasse 26, 8010 Graz, Austria
e-mail: bernd.kaufmann@uni-graz.at

Introduction and previous work

The Rhaetian reefs (the so-called 'Oberrhät-Riffe') of the Northern Calcareous Alps have been subjected to

investigations of stratigraphy, facies, and palaeoecology for many years (e.g. Zankl 1969; Schäfer 1979; Piller 1981; Stanton and Flügel 1989; Bernecker et al. 1999). Diagenetic studies have received less attention but were nevertheless carried out by several authors (e.g. Mirsal and Zankl 1979; Mazzullo et al. 1990; Satterley et al. 1994; Flügel and Koch 1995).

Due to its position at the platform margin, the Steinplatte complex, situated 40 km W of Adnet, is well comparable to the reefal limestones of Adnet in terms of palaeogeography and facies (Piller 1981; Stanton and Flügel 1989). Its diagenetic evolution was discussed by Mazzullo et al. (1990) who focused on the diagenesis of RFCs and provided evidence for subaerial exposure at the Triassic–Jurassic boundary. Flügel and Koch (1995), based merely on petrographic observations, described cyclic changes of marine and meteoric diagenesis that were interpreted as the result of periodic emergence and submergence of the Steinplatte area during Rhaetian times. The Wilde Kirche reef complex (near Innsbruck, Tyrol), an isolated reef structure within the Kössen Basin, was the aim of a diagenetic study of Satterley et al. (1994) based on petrographic and geochemical analyses. In the latter study, a phase of emergence was observed at the Triassic–Jurassic boundary immediately prior to the drowning of the Dachstein carbonate platform.

The first examinations of the reefal limestones of Adnet near Hallein (Salzburg) related to diagenesis were performed by Flügel and Tietz (1971) who examined the causes for the red colour of internal sediments. They concluded that this phenomenon is related to oxidized insoluble residues of the carbonate host rock which were deposited in cavities, the staining Fe being due to goethite and Fe-hydroxides. Mirsal and Zankl (1979) analyzed the geochemistry including carbon and oxygen isotopes of void-filling calcite cements of the Adnet reef and the Feichtenstein reef complex (12 km E of Adnet), the latter situated within the Kössen Basin. These authors interpreted geochemical variations of calcite cements as being caused by changing salinity in a gradually closing system.

The subject of the present study is the elaboration of the syn- and post-Rhaetian diagenetic evolution of the reefal limestones of Adnet (in the following called 'Adnet reef') by means of petrographic and geochemical methods. It is a contribution to the knowledge of the overall diagenetic evolution of Rhaetian reefs and its controlling factors. The Adnet reef reveals an unusual manifold early diagenesis characterized by a dissolution phase (karstification) followed by phases of cementation and internal sedimentation. It thus offers an excellent opportunity to examine the reefal development and the early diagenesis depending on relative sea-level changes. It can also be expected that the diagenetic sequence reflects the latest Rhaetian to Early Jurassic basinal development. Investigations focused on strata immediately below the Triassic–Jurassic boundary in order to obtain insights on a long phase of emergence at this time.

Palaeogeographic setting

The Northern Calcareous Alps, a part of the Austroalpine nappe complex, are the northernmost overthrusted part of the eastern Alps. They form a W to E-striking, 500-km-long and 20 to 50-km-wide thrust belt that extends from Bregenz in the west to Vienna in the east (Mandl 2000) (Fig. 1a).

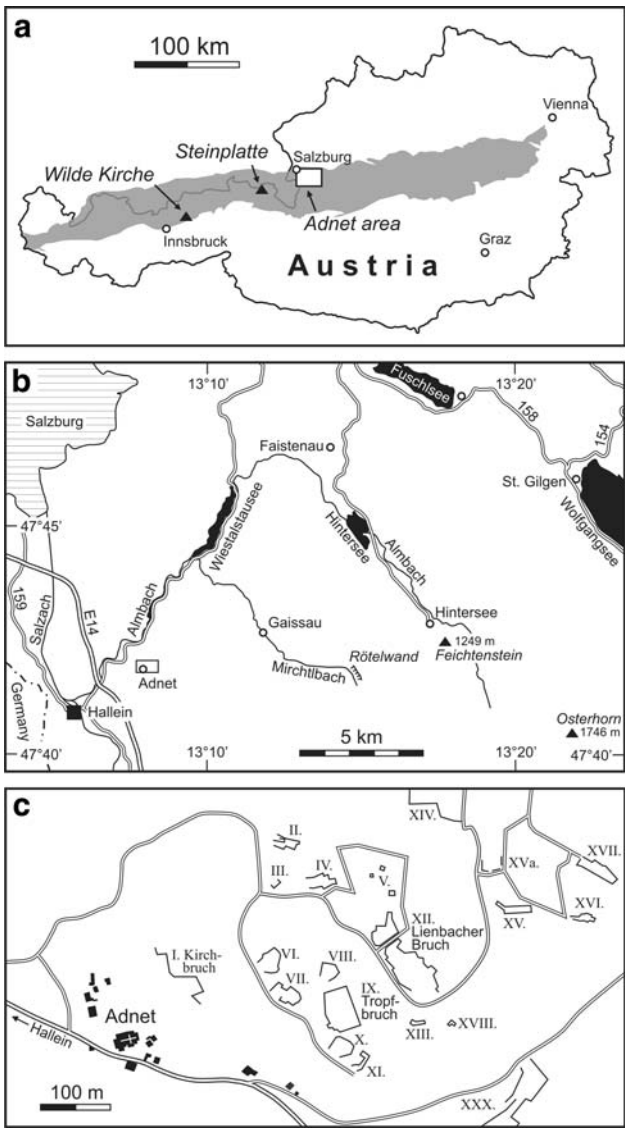

Fig. 1 Locality maps. **a** Location of the Adnet area (*box* indicates area of **b**) and other Rhaetian reefs (Steinplatte, Wilde Kirche) which were studied by Mazzullo et al. (1990) and Satterley et al. (1994). *Shaded* area marks the extension of the Northern Calcareous Alps. **b** Map of the Adnet area SE of Salzburg. *Box* indicates area of **c**. **c** Location of the Adnet quarries (redrawn from Kieslinger 1964)

During Late Triassic times, the Northern Calcareous Alps were part of an extensive, up to 300-km-wide shelf at the passive continental margin of the northwestern Neotethys (Haas 1991), situated about 30° north of the equator (Marcoux et al. 1993). Tropical conditions and low sea level favoured the establishment of giant, up-to-1,200-m thick, carbonate platforms (Loferer and Leoganger Steinberge, Steinernes Meer, Hochkönig, Tennengebirge, Dachstein Mountains, Totes Gebirge, Hochschwab, Hohe Wand) composed essentially of Hauptdolomit and Dachstein Limestone. Rhythmic successions in the Dachstein Limestone comprising subaerial to shallow subtidal deposits are well known as "Lofer Cyclothems" (Fischer 1964). The southern and southwestern, ocean-faced margins of the carbonate platforms (e.g. Hoher Göll, Hochkönig, Gosaukamm) were rimmed by thick reefal carbonates formed by massive Dachstein Limestone (e.g. Zankl 1969; Satterley et al. 1994; Wurm 1982). The transition into the pelagic realm of the Hallstatt facies was often characterized by rather steep slopes with evidence for synsedimentary tectonics (Zankl 1971).

With the onset of the Rhaetian, the Kössen Basin was formed in the northern part of the Hauptdolomit/Dachstein carbonate shelf. Carbonate buildups like the Steinplatte complex (Piller 1981; Stanton and Flügel 1989) and the Adnet reef (Schäfer 1979; Bernecker et al. 1999; this study) developed at the transition between this intrashelf basin and the Dachstein carbonate platform. These Rhaetian reefs ('Oberrhätriffe') are the first "modern" reefs in earth history in terms of being dominated by scleractinian corals. Reefal and shallow carbonate platform sedimentation was terminated at the end of the Rhaetian when the whole Austroalpine carbonate shelf was affected by subaerial exposure (Mazzullo et al. 1990; Satterley et al. 1994; Bernecker et al. 1999). Subsequent drowning occurred in the Early Jurassic when shallow pelagic marine ammonite-bearing limestones (e.g. Adnet Formation) were deposited (Böhm 1992).

Stratigraphic setting of the Adnet reef

The limestone quarries near the village of Adnet are situated about 10 km SE of Salzburg (Austria) (Fig. 1). In the Tropfbruch quarry (Fig. 1c), the core of an Upper Rhaetian reef with meter-sized colonies of the coral *Retiophyllia* is exposed (Fig. 2). This reef forms the uppermost 6 m of the so-called 'Oberrhätkalk', which has an overall thickness of ca. 150 m (Kramer and Kröll 1979). Individual reef stages, unconformities, depth of karst dissolution, and sea-level changes have been examined by Bernecker et al. (1999). Two unconformities prior to and one at the Triassic–Jurassic boundary were interpreted as the result of repeated end-Triassic subaerial exposure and karstification. The Triassic–Jurassic boundary is, however, not exposed in this quarry but is assumed a few meters above the topmost part of the outcrop. This is suggested by neptunian dikes filled with red Lower Jurassic sediments. The Triassic–Jurassic boundary is exposed in the adjacent Lienbacher Bruch (Fig. 1c).

The 'Oberrhätkalk' correlates stratigraphically with the Eiberg Member of the Kössen Beds and the Adnet reef is thus positioned in the *Choristoceras marshi* ammonoid zone and in the *Misikella posthernsteini* conodont extinction zone (Fig. 3). Due to the lack of outcrops, it is not clear whether the Oberrhätkalk of Adnet has a direct connection to the Dachstein carbonate platform or if it represents an isolated reef complex within the Kössen Basin as was proved for the nearby Rötelwand reef (Schäfer 1979) and the Feichtenstein reef complex (Mirsal and Zankl 1979). At the end of the Rhaetian, the Adnet

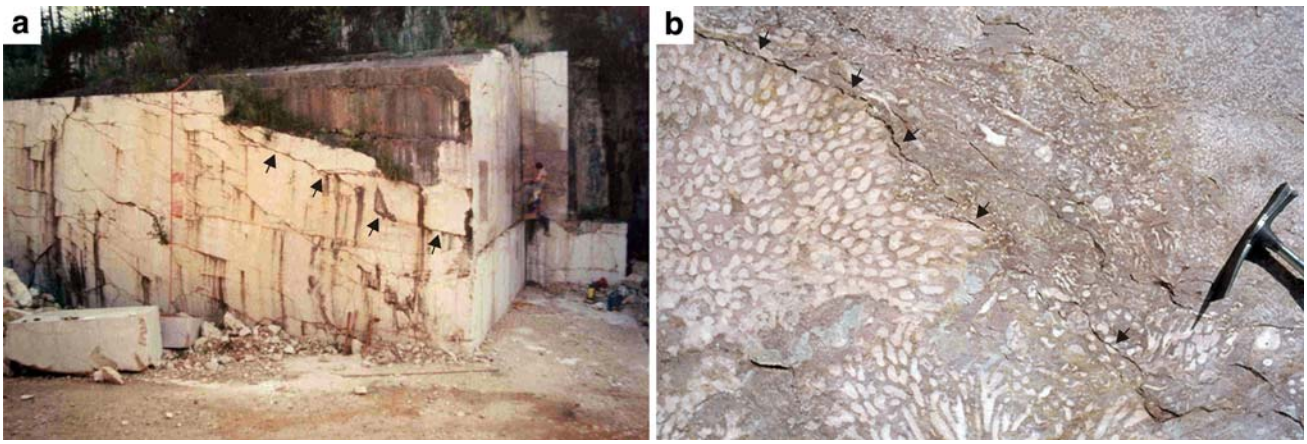

Fig. 2 Tropfbruch quarry at Adnet (near Salzburg, Austria). **a** Sawed quarry walls. Height of quarry wall is 6 m (see persons on the right for scale). *Arrows* mark intra-Rhaetian unconformity A (Bernecker et al. 1999). **b** *Retiophyllia* colony bordered at the top by intra-Rhaetian unconformity (*arrowed*)

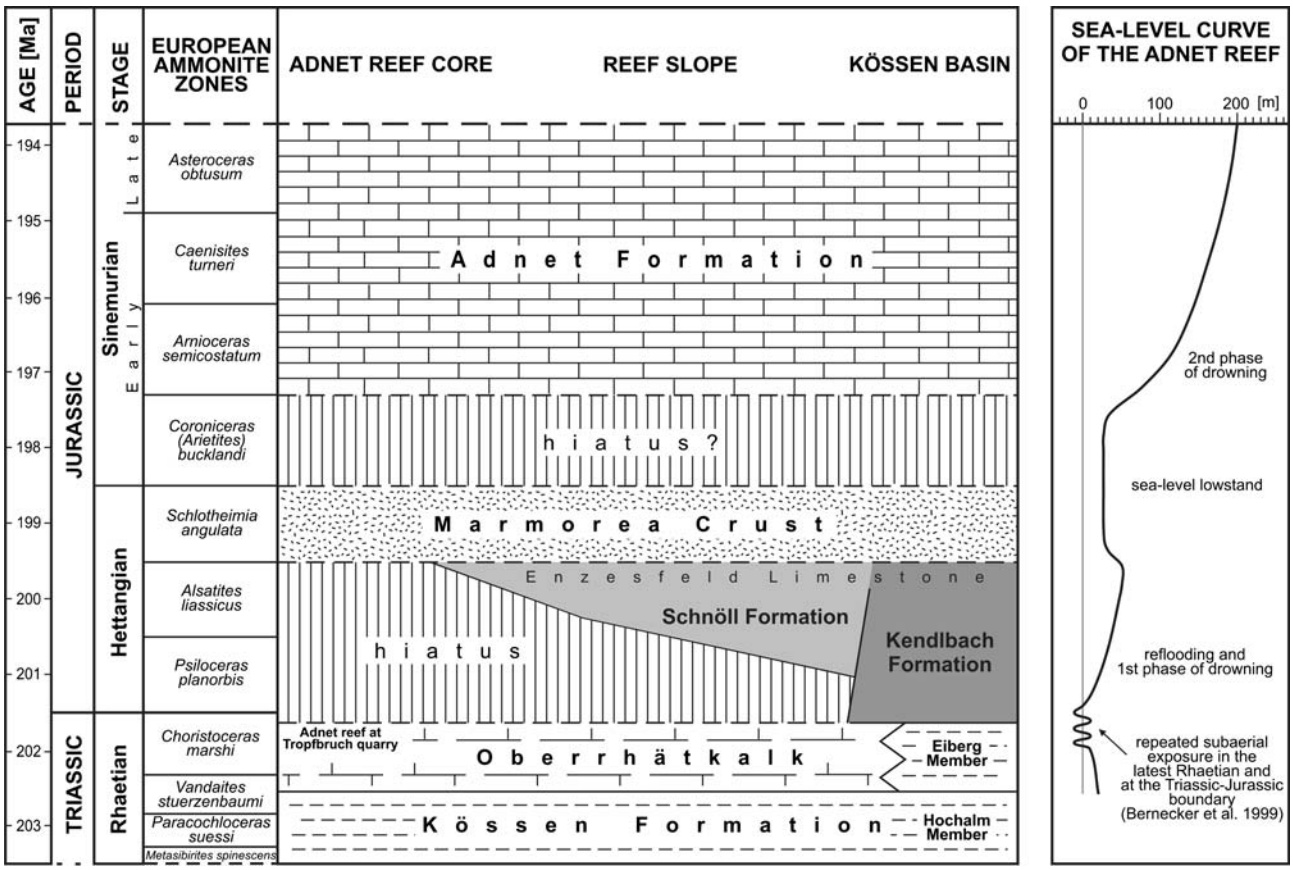

Fig. 3 Chronostratigraphic framework of Rhaetian to Sinemurian strata of the Adnet area based mainly on Kramer and Kröll (1979), Böhm et al. (1999), and Krystyn et al. (2005). Stratigraphic range of the 'Marmorea Crust' and earliest Sinemurian hiatus is uncertain. Stratigraphic range of the Adnet reef is exaggerated. Ages of the Triassic–Jurassic and Hettangian–Sinemurian boundaries after Pálfy (2008)

reef had a relief of 50–80 m with a 10–15° north to northeast slope towards the basinal sediments of the Kössen Formation (Böhm et al. 1999). Hettangian to Sinemurian (Lower Jurassic) strata progressively onlap the Adnet reef with the hiatus increasing in direction to the reef core at the Tropfbruch quarry (Böhm et al. 1999) (Fig. 3). The toe of the reef slope and the transition to the basinal Kössen Beds (Eiberg Member) is conformably overlain by the Lower Hettangian Kendlbach Formation. The middle to lower reef slope is covered by the coloured micritic limestones of the Upper Hettangian Schnöll Formation (Böhm et al. 1999). Finally, the upper reef slope is bordered unconformably by an Upper Hettangian ferromanganese crust ('Marmorea Crust') followed above by red crinoid-rich biomicrites of the Lower Sinemurian Adnet Formation (Böhm et al. 1999) (Fig. 3).

Methods

All samples were collected from the uppermost part of the Tropfbruch quarry below the Triassic–Jurassic boundary where bioclastic grainstones with isolated *Retiophyllia* colonies occur. Samples were taken from a Pleistocene karst surface in the non-exploited part of the quarry. In addition, an oriented sample was obtained from a neptunian dike in the quarry wall that was filled with red biomicrites derived from the Lower Sinemurian Adnet Formation.

Petrography was studied in 38 large thin sections (6 × 9 cm). Staining was performed on all thin sections using Alizarin Red S and potassium ferricyanide to distinguish between calcite and dolomite and for a semi-quantitative estimation of Fe contents. Cathodoluminescence (CL) was conducted on a CITL cold cathode luminescence (CCL) 8200 mk4 operating under 20 kV accelerating voltage, 300-μA beam current, and a beam diameter of 10 mm. Seven thin sections were subjected to 250 analyses of cation compositions (Ca, Mg, Sr, Mn, and Fe) with the aim to refer geochemical analyses directly to CL characteristics of neomorphically altered coral skeletons, internal sediments and calcite cements. These analyses were carried out by a CAMECA Camebax-microbeam wavelength-dispersive microprobe operating under 20 kV accelerating voltage and 16 to 22-nA beam current with a 5 to 10-μm spot size.

Approximate detection limits were 100 ppm for Ca and Mg, 200 ppm for Sr, and 300 ppm for Mn and Fe. The confidential intervals at 95% (2σ) were ±200 ppm for all element values between absolute detection limit and 10,000 ppm, ±0.2 wt% for all element values between 1.0 and 10.0 wt%, and ±0.35 wt% for all element values above 10.0 wt%.

Stable-isotope ratios were measured in 27 calcite microsamples (>30 ng) extracted by a 400-µm-thick dental drill. Samples were prepared with anhydrous phosphoric acid in an automatic carbonate reaction device (Carbo-Kiel) attached to a Finnigan MAT 252 mass spectrometer. Isotopic ratios were corrected for ^{17}O contribution and are reported in ‰ relative to the PDB standard. Precision was monitored through analyses of the NBS 18, 19, and 20 calcite standards and is between 0.01 and 0.03% for both carbon and oxygen-isotope compositions.

Diagenetic sequence in dissolution cavities

The diagenetic history of the Adnet reef exposed in the Tropfbruch quarry is unraveled by conventional petrographic, CL and geochemical investigations of neomorphic spar, carbonate cements and internal sediments preserved in dissolution cavities. These cavities originated from partly or complete dissolution of aragonitic coral skeletons (*Retiophyllia*) and display very variable diagenetic successions (Table 1). Despite these small-scale variations, a superordinate diagenetic sequence is present in almost all investigated samples (Fig. 4): septa of coral skeletons [Fig. 4(1)] were transformed into *neomorphic calcite spar* [Fig. 4(2)], which in turn is sparsely overgrown by *dog-tooth cement I* [Fig. 4(3)]. The pore space is subsequently filled with grey *internal sediment I* (IS I) whose individual layers are often bounded by ferromanganese crusts [Fig. 4(4)]. *Syntaxial cements* are observed on echinoderm remains of IS I. Radiaxial-fibrous calcites (RFCs) form isopachous seams on internal sediments and at cavity walls [Fig. 4(5)] and are followed by a thin zone of *dog-tooth cement II* [Fig. 4(6)]. The red *internal sediment II* (IS II) is only locally present and postdates IS I and RFCs. The remaining pore space, if present, is filled with slightly ferroan, zoned *blocky calcite cement* [Fig. 4(7)], which is sometimes displaced by *saddle dolomite* [Fig. 4(8)]. Petrographic, CL, and geochemical characteristics (carbon and oxygen isotopes; Ca, Mg, Sr, Mn, and Fe concentrations) of all diagenetic products are shown in Table 2.

Neomorphic calcite spar

Neomorphic calcite spar has replaced and traced relics of septa of aragonitic *Retiophyllia* corallites, which escaped former dissolution (Fig. 5a). Its fabric is a mosaic of

Table 1 Selected examples of diagenetic sequences observed within dissolved *Retiophyllia* corallites showing the variety of temporal and spatial successions

Example 1	Example 2	Example 3	Example 4	Example 5	Example 6
Aragonite leaching/ neomorphism	Aragonite leaching/ neomorphism	Aragonite leaching/neomorphism	Aragonite leaching/ neomorphism	Aragonite leaching/ neomorphism	Aragonite leaching/ neomorphism
Dog-tooth cement I	Dog-tooth cement I	Biomicritic IS I with echinoderm remains + ferromanganese crusts	Dog-tooth cement I	Dog-tooth cement I	Dog-tooth cement I
Biomicritic IS I	Biomicritic IS I with echinoderm remains	Biomicritic IS I	Biomicritic IS I with ferromanganese crusts	Micritic IS I	Biomicritic IS I
Radiaxial-fibrous calcite	Micritic IS I + crystal silt	Radiaxial-fibrous calcite	Pelmicritic IS I	Radiaxial-fibrous calcite	Pelmicritic IS I
Dog-tooth cement II	Biomicritic IS II with ostracods	Corrosion of radiaxial-fibrous calcite	Radiaxial-fibrous calcite	Biomicritic IS I with echinoderm remains	Biomicritic IS I with echinoderm remains
Blocky calcite cement	–	Biomicritic IS I	Dog-tooth cement II	Radiaxial-fibrous calcite	Syntaxial cement
Saddle dolomite	–	Radiaxial-fibrous calcite	Pelmicritic IS I	Micritic IS I	Radiaxial-fibrous calcite
–	–	Blocky calcite cement	Blocky calcite cement	Radiaxial-fibrous calcite	Dog-tooth cement II
–	–	–	–	Biomicritic IS II	Blocky calcite cement
–	–	–	–	–	Corrosion of blocky calcite cement
–	–	–	–	–	Crystal silt

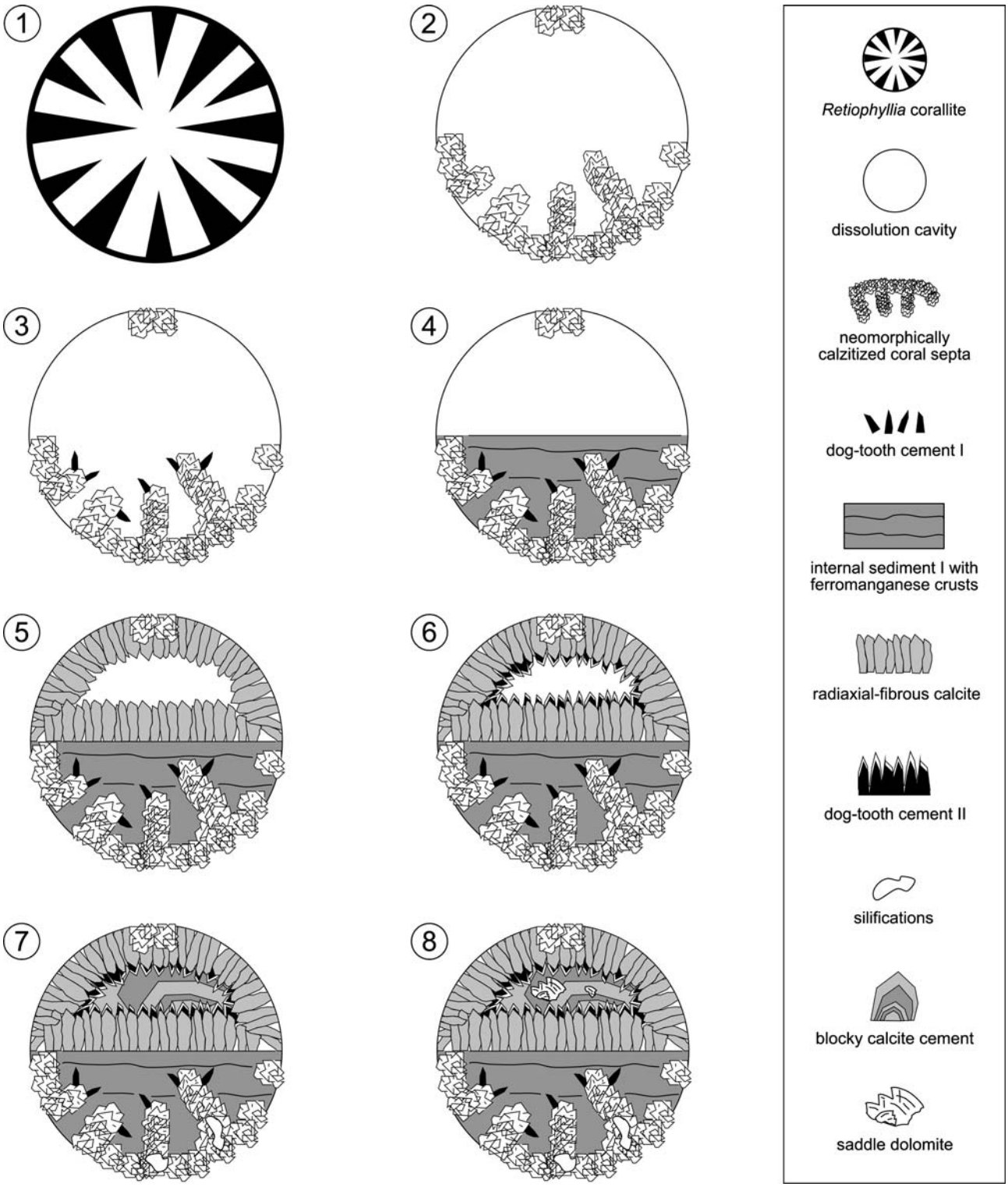

Fig. 4 Superordinate diagenetic sequence preserved in molds of *Retiophyllia* corallites of the Tropfbruch quarry

equant, anhedral crystals with grain sizes of 10–40 μm (micro- to pseudospar). Neomorphic calcite spar is composed of low-Mg calcite (LMC) with a $MgCO_3$ content of 0.1–1.9 mole%. It is nonluminescent with few orange domains up to completely mottled, dull-orange (Fig. 5b). Concentrations of Sr, Mn, and Fe range from below detection limit (70% of all analyses) to 530, 1,550, and 3,050 ppm, respectively. Elevated Mn and Fe values are

Table 2 Occurrence, petrography, CL pattern, and geochemistry of diagenetic products within dissolution cavities of the Adnet reef

Diagenetic product	Neomorphic calcite spar	Dog-tooth cement I	IS I	Syntaxial cement	Radiaxial-fibrous calcite (RFC)	Crystal silt	IS II	Dog-tooth cement II	Microdolomite inclusions	Chalcedony/ microquartz	Blocky calcite cement	Saddle dolomite
Occurrence	Replacing septa of *Retiophyllia* corallites	Sparsely overgrowing neomorphic calcite spar	Postdating neomorphic calcite spar and dog-tooth cement I	On echinoderm fragments of IS I	Nucleating on neomorphic calcite spar and IS I	In *Retiophyllia* biomolds and vugs	Postdating RFCs	Syntaxially overgrowing RFCs	Within RFCs, crinoidal fragments, dog-tooth cement II, and syntaxial cements	Within *Retiophyllia* corallites; at RFC crystal boundaries	Postdating RFCs and dog-tooth cement II	Postdating blocky calcite cement
Fabric	Pseudomorph	Single crystals growing irregularly from the coral septa in all directions	Micritic to peloidal with some fine-grained bioclasts	Syntaxial	Isopachous cement rims	Crystal debris from corrosion of RFCs	Micritic with coarse grained bioclast, e.g. crinoids, mollusks	Irregular rims	Scattered, "porphyrotopic"	Replacive	Void-filling cement	Replacive or void-filling cement
Crystal shape	Equant-anhedral	Euhedral (acute rhombohedron to acute scalenohedron)	–	An- to euhedral with microdolomite inclusions	Euhedral, bladed to fibrous; rarely corroded crystal tips	Anhedral	–	Euhedral, equant-obtuse to acute skalenohedrons	Sub- to euhedral	Irregular, nodular, spheroidal	Equant, an- to subhedral, enfacial junction	Sub- to euhedral, curved, saddle-like habit
Crystal size	10–40 μm	30–50 μm	–	0.3–1.2 mm	2.0–4.0 mm	10–40 μm	–	Up to 250 μm	Up to 10 μm	Coarse to very coarse (600–3,000 μm)	0.1–4.0 mm	200–300 μm
Colour/stain[1]	Clear/red	Clear/red	Light grey to beige/red	Clear/red	Cloudy/red	Clear to brownish/ red	Reddish brown/ red	Clear/red	Clear/no stain	Dirty whitish/ no stain	Clear/red with blueish growth zones	Cloudy/no stain
CL	Nonluminescent to mottled dull-orange	Nonluminescent	Mottled bright-yellow	Nonluminescent to mottled dull-orange	Zoned nonluminescent and mottled bright-yellow	Dull	Mottled dull	Nonluminescent with a bright outer zone	Dull red	Nonluminescent	Bright to dull, homogeneous to zoned	Dull red
Mole% $CaCO_3$	97.9–99.6	97.7–99.2	–	99.5–99.6	97.0–99.5	–	–	97.8–99.9	52.0–55.6	–	97.9–99.9	–
Mole% $MgCO_3$	0.1–0.9	0.8–2.3	–	0.3–0.5	0.2–2.9	–	–	0.01–2.1	44.3–48.0	–	0.02–1.0	–
Sr^{2+} (ppm)	b.d.l.–530	250–690	–	420–510	Nonluminescent: b.d.l.–890 mottled yellow: b.d.l.–650	–	–	Nonluminescent: b.d.l.–660 yellow: b.d.l.–490	b.d.l.–400	–	b.d.l.–630	–
Mn^{2+} (ppm)	b.d.l.–1,550	b.d.l.	–	b.d.l.	Nonluminescent: b.d.l.–350 mottled yellow: b.d.l.–2,760	–	–	Nonluminescent: b.d.l.–830 yellow: 1,070–6,260	b.d.l.–950	–	b.d.l.–5,850	–
Fe^{2+} (ppm)	b.d.l.–3,050	b.d.l.–1,630	–	b.d.l.	Nonluminescent: b.d.l.–730; mottled yellow: b.d.l.–6,080	–	–	Nonluminescent: b.d.l.–400; yellow: b.d.l.–470	b.d.l.–990	–	b.d.l.–840	–
$\delta^{18}O$ PDB	−1.7 (±0.5)	–	−3.0 (±0.4)	–	−1.3 (±0.7)	–	–0.8 (±0.4)	–	–	–	−5.7 (±0.1)	–

Table 2 continued

Diagenetic product	Neomorphic calcite spar	Dog-tooth cement I	IS I	Syntaxial cement	Radiaxial-fibrous calcite (RFC)	Crystal silt	IS II	Dog-tooth cement II	Microdolomite inclusions	Chalcedony/ microquartz	Blocky calcite cement	Saddle dolomite
δ^{13}C PDB	+2.9 (±0.3)	–	+2.7 (±0.3)	–	+2.4 (±0.1)	–	+2.5 (±0.4)	–	–	–	+2.8 (±0.1)	–
Diagenetic environment	meteoric–phreatic	Meteoric– or mixed meteoric-marine–phreatic	Marine-phreatic					Shallow burial		Deeper burial, hydrothermal influences		

[1] Alizarin Red S and potassium ferricyanide, *b.d.l.* below detection limit

Fig. 5 Diagenetic products of the Adnet reef. **a** Transmitted-light view of recrystallized *Retiophyllia* corallite. Relics of individual septa can be recognized by micrite seams (*arrowed*). **b** CL view of **a** displays nonluminescent to mottled coral septa (*arrowed*). **c** Transmitted-light view of neomorphically calcitized coral septa overgrown by irregularly growing dog-tooth cement I. **d** CL view of nonluminescent dog-tooth cement I (*arrowed*) nucleating on mottled-luminescent coral septa. **e** Transmitted-light view of internal sediment I (IS I), cross-bedded at the top. Note ferromanganese crust (*arrowed*). **f** Transmitted-light view of internal sediment II (IS II) derived from the Lower Sinemurian Adnet Formation containing crinoid ossicles, gastropods, foraminifers, sponges, ostracods, and pelecypods. **g** Crossed-nicols view of selective silification (in the centre of the photograph) in *Retiophyllia* corallite

found in regions of mottled dull-orange CL, whereas low values correspond to areas with nonluminescence. Stable-isotope analyses of four samples show mean values of $\delta^{18}O = -1.7$ (±0.5)‰ and $\delta^{13}C = +2.9$ (±0.3)‰ (Fig. 6).

Micro- to pseudosparitic texture, relics of primary structures and the inhomogeneous mottled CL rather argue for neomorphic alteration than for dissolution and subsequent cementation. Low Sr values suggest stabilization in an open system by meteoric waters. Varying, partly increased Mn and Fe contents characterize reducing redox conditions in a deeper level of a meteoric–phreatic environment. However, stable-isotope values plot in or very near to the field of the Rhaetian seawater composition indicating negligible alteration (Fig. 6).

Dog-tooth cement I

Dog-tooth cement I is the first cement precipitated on neomorphic calcitized septa of *Retiophyllia* corallites and in dissolution cavities (Fig. 5c). Scattered scalenohedral crystals are 30–50 μm in length, inclusion-free, and irregularly growing in different directions on the substratum. Dog-tooth cement I is nonluminescent (Fig. 5d) and composed of LMC with $MgCO_3$ contents of 0.8–2.3 mole%. Sr concentrations are between 250 and 690 ppm, Mn and Fe concentrations are mostly below the detection limit of the microprobe. Unfortunately, crystals of dog-tooth cement I were too small to be sampled by conventional methods for stable-isotope analyses.

Dog-tooth cements (also referred to as scalenohedral cements) can form under different diagenetic conditions (Reinhold 1999). They show significantly varying characteristics allowing the attribution to distinct diagenetic environments. The occurrence of dog-tooth cement I as first cement generation in dissolution cavities and on the substratum of neomorphically altered coral skeletons points to early formation in a marine (or possibly mixed meteoric-marine) environment subsequent to a meteoric phase. Dog-tooth cement I was probably precipitated as stable LMC, as indicated by the unaltered crystal habit, low

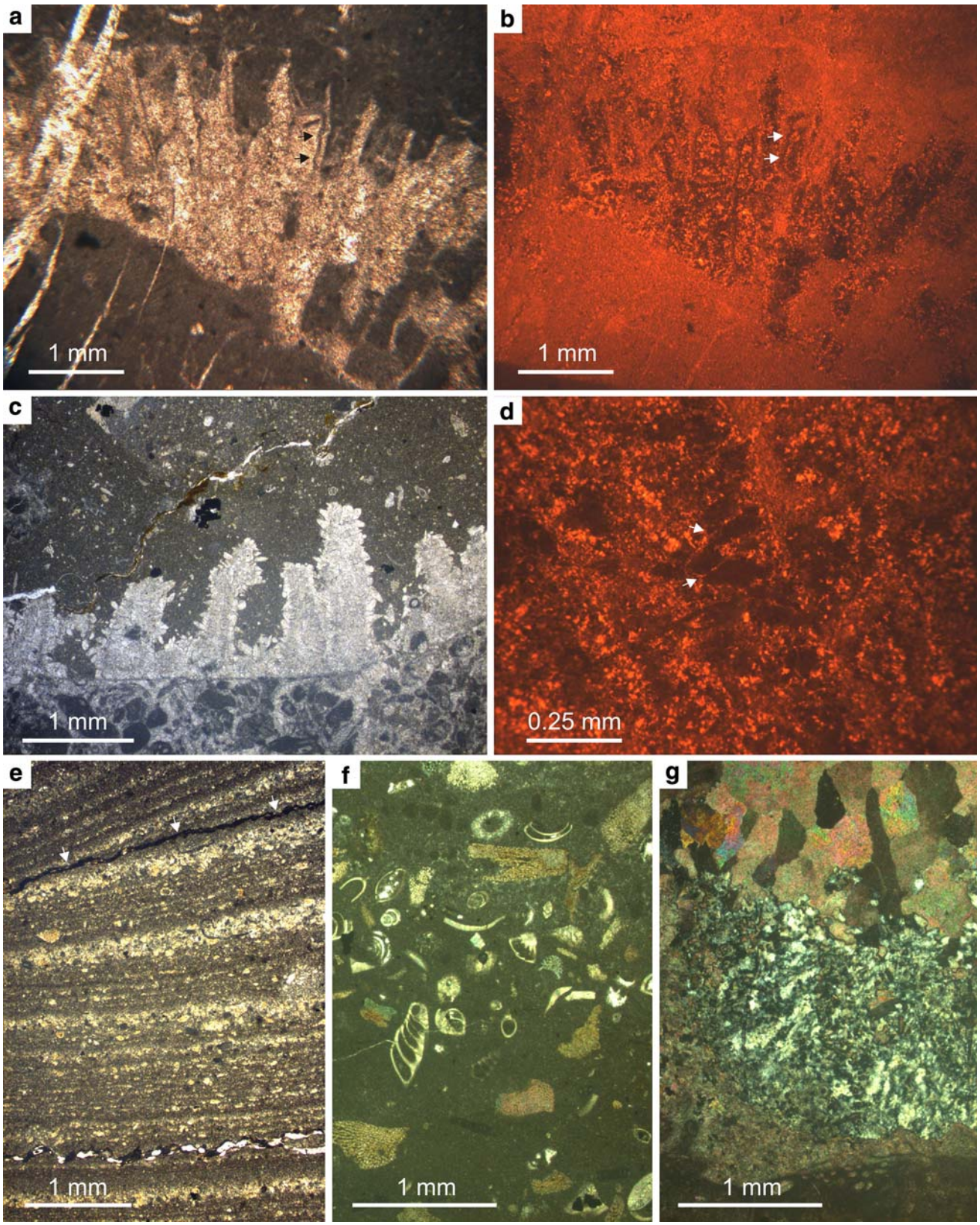
a
1 mm
b
1 mm
c
1 mm
d
0.25 mm
e
1 mm
f
1 mm
g
1 mm

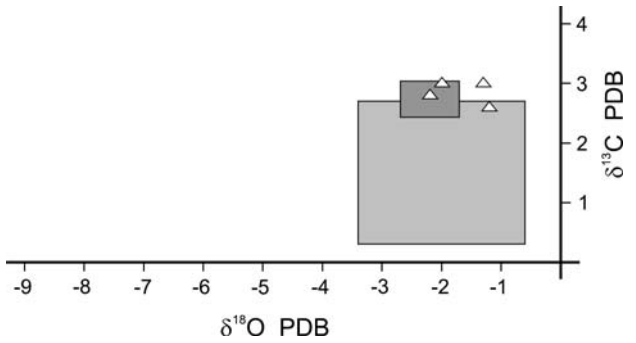

Fig. 6 $\delta^{18}O$ and $\delta^{13}C$ plots of neomorphic calcite spar of the Adnet reef. *Shaded rectangle* indicates field of Rhaetian seawater composition (*light grey* Korte et al. 2005; *dark grey* Mazzullo et al. 1990)

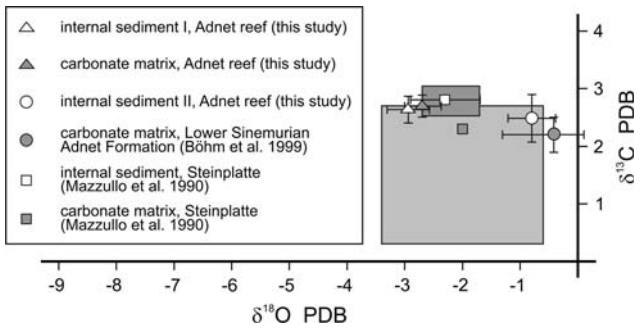

Fig. 7 $\delta^{18}O$ and $\delta^{13}C$ plots of internal sediments and carbonate matrix of Upper Rhaetian reef limestones and the Lower Sinemurian Adnet Formation. *Bars* show spread of values. *Shaded rectangle* indicates field of Rhaetian seawater composition (*light grey* Korte et al. 2005; *dark grey* Mazzullo et al. 1990)

Mg content, and the absence of microdolomite inclusions. Nonluminescene and low Mn and Fe concentrations indicate precipitation from oxidizing pore water. The low Mg content and the scattered occurrence of crystals points to precipitation under conditions with lower rates of fluid flow and lower availability of CO_3^{2-} ions (Given and Wilkinson 1985).

Internal sediment I

Internal sediment I (IS I) postdates dog-tooth cement I and mostly predates RFCs (Fig. 5e). It is grey in colour (beige weathering), geopetally layered, sometimes cross-bedded, and consists of micritic or peloidal sediments with fine-grained skeletal and siliciclastic debris. Individual layers are often separated by ferromanganese crusts. CL is mottled orange. Stable-isotope analyses of five samples show mean values of $\delta^{18}O = -3.0$ (±0.4)‰ and $\delta^{13}C = +2.7$ (±0.3)‰ (Fig. 7).

Geopetal, internal deposition of biomicritic and peloidal sediments indicates an influx of IS I under marine-phreatic conditions. The partly observed cross-bedding argues for varying pore geometry and possibly changing hydrodynamic conditions in the pore spaces. IS I is probably derived from karstification and erosion of the Rhaetian reef limestone. This assumption is supported by the similarity of stable-isotope values of IS I compared to three reference values ($\delta^{18}O = -2.7$ (±0.3)‰; $\delta^{13}C = +2.7$ (±0.2)‰) of the reefal carbonate matrix (Fig. 7). The same interpretations were made by Mazzullo et al. (1990) and Satterley et al. (1994) who reported carbonate-depleted internal sediments from the Steinplatte and Wilde Kirche, respectively. These internal sediments exhibit, in addition to similar stable-isotope values (Fig. 7), the same mineralogical composition of the insoluble residues of internal sediments and the surrounding host rock (Mazzullo et al. 1990). IS I was probably deposited during renewed flooding of the Adnet reef in Early to Mid-Hettangian times. Ferromanganese crusts separating individual layers indicate a stepwise internal sedimentation interrupted by phases of omission.

Syntaxial cement

Syntaxial cement is locally developed on echinoderm remains of IS I (Fig. 8b). Crystals are often rhombohedral and vary in size between 0.3 and 1.2 mm. Microdolomite inclusions are common. Syntaxial cement displays either nonluminescence or a mottled dull-orange CL, microdolomites luminesce red. Mineralogically, it is composed of LMC with $MgCO_3$ contents of 0.3–0.5 mole%. Sr concentrations are between 420 and 510 ppm, Mn and Fe concentrations are always below the detection limit. As in dog-tooth cements, crystals of syntaxial cement are too small to be sampled for stable isotopes.

Microdolomite inclusions in syntaxial cements indicate an original HMC mineralogy (see also 'RFC' below). Low Mn and Fe concentrations indicate formation in an oxidizing environment.

Radiaxial-fibrous calcite

Radiaxial-fibrous calcite (RFC) overgrows neomorphically calcitized coral septa or nucleates on IS I. It forms 2 to 4-mm-thick isopachous layers of bladed or fibrous, cloudy crystals (Fig. 8a, c). Subordinate thin layers are often interrupted by thin coatings of pelmicritic internal sediment. RFC crystals usually diverge away from their substratum and display the characteristic undulose extinction, convergent c axes and curved twins (Fig. 8a). Turbidity of crystals is caused by microdolomite inclusions which are subhedral to euhedral in shape and up to 10 μm in size. Crystal terminations of RFCs are sometimes corroded (see also 'Neptunian dikes') and overlain by crystal silt consisting of eroded crystal fragments (Fig. 8a). RFC has

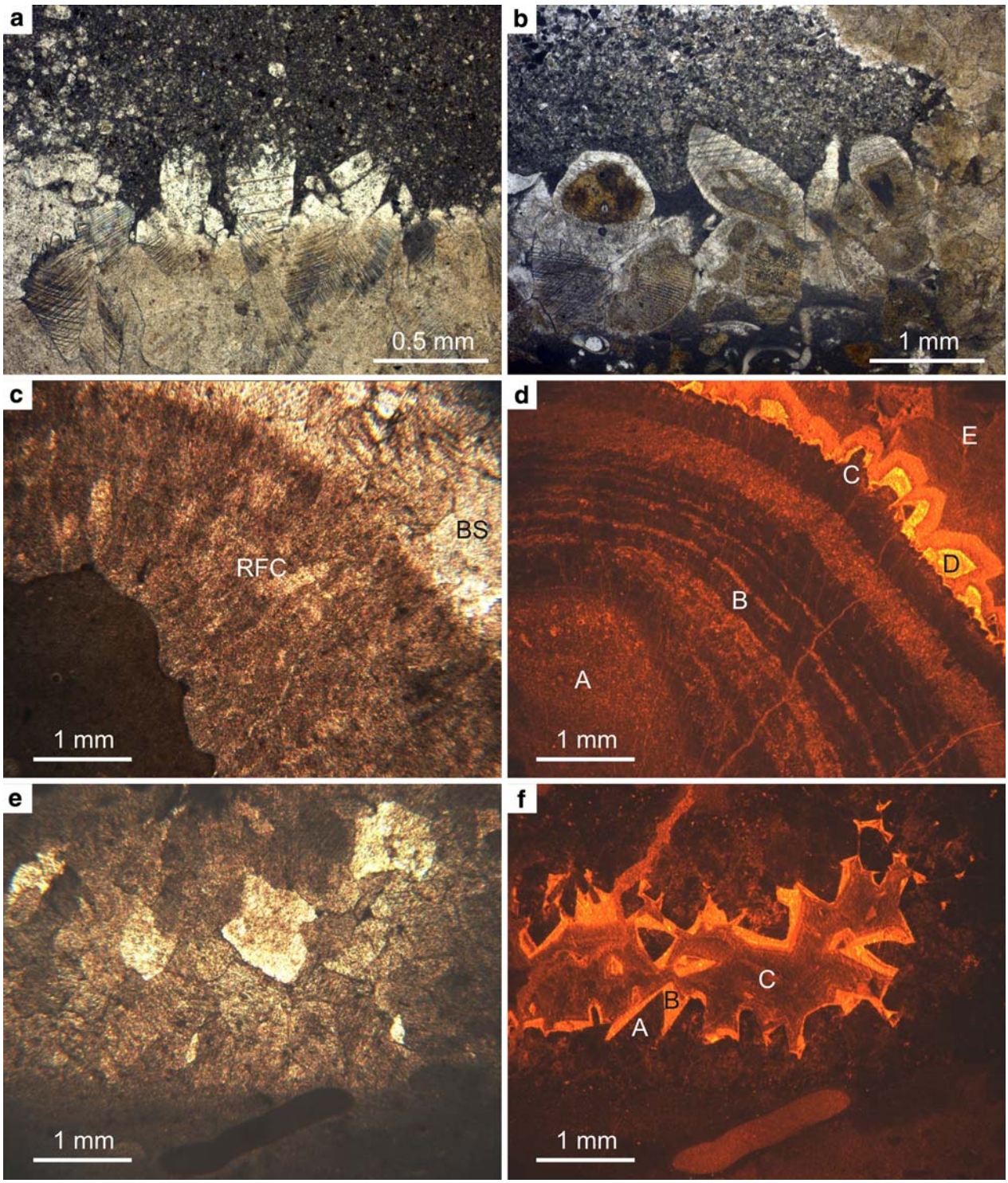

Fig. 8 Diagenetic products of the Adnet reef. **a** Transmitted-light view of radiaxial-fibrous calcite (*RFC*) with corroded crystal tips overlain by crystal silt. Note curved twins and brownish turbidity, the latter caused by microdolomite inclusions. **b** Transmitted-light view of syntaxial cements overgrowing crinoid ossicles. Note optic continuity (continuous cleavage). **c** Transmitted-light view of isopachous seam of brownish-turbid radiaxial-fibrous calcite (*RFC*) overlain by clear, equant blocky spar (*BS*). **d** CL view of **c** reveals mottled-luminescent micrite matrix (*A*) followed by irregularly alternating nonluminescent and mottled-luminescent RFC layers (*B*) overgrown by nonluminescent dog-tooth cement II (*C*) with bright- and moderate-luminescent outer zones (*D*). Remaining pore space is filled by dull-luminescent, ferroan blocky spar (*E*). **e** Transmitted-light view of dissolution cavity, showing equant, blocky calcite cement. **f** CL view of **e** reveals nonluminescent dog-tooth cement II (*A*) with bright-luminescent outer margins (*B*). Central void space is occluded by ferroan, dull-luminescent blocky spar (*C*)

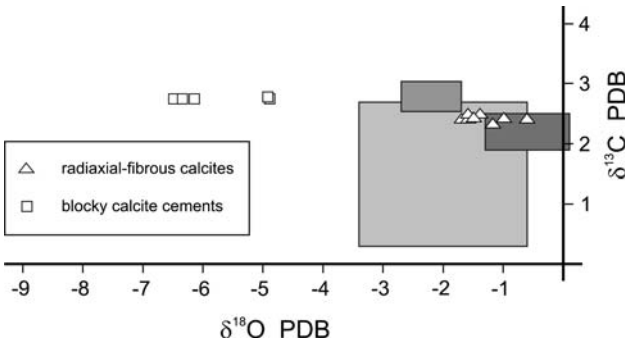

Fig. 9 $\delta^{18}O$ and $\delta^{13}C$ plots of radiaxial-fibrous calcites and blocky calcite cements of the Adnet reef. *Shaded rectangles* indicate fields of Rhaetian (*light grey* Korte et al. 2005; *medium grey* Mazzullo et al. 1990) and Sinemurian (*dark grey* Böhm et al. 1999) seawater composition

extremely varying $MgCO_3$ contents of 0.3–8.5 mole%. CL is mottled yellow at the base of crystals changing to the top to nonluminescene or alternating (7–15 zones) with wide zones of nonluminescene and thin zones of mottled yellow CL (Fig. 8d). Sr concentrations are between <200 and 650 ppm. Mn and Fe concentrations are mostly below the detection limit but may attain, in zones of mottled yellow CL, 2,760 and 6,080 ppm, respectively. Stable-isotope values of RFCs have been obtained from eight samples and show mean values of $\delta^{18}O = -1.3$ (±0.7)‰ and $\delta^{13}C = +2.4$ (±0.1)‰ (Fig. 9). Areas of nonluminescence are diagenetically unaltered and correspond to the heaviest oxygen-isotope values ($\delta^{18}O = -0.6$ to -1.2‰).

Radiaxial-fibrous calcites are precipitated post-sedimentary as indicated by their occurrence in dissolution cavities and their position in the diagenetic sequence. Isopachous layers of RFCs characterize a pore space completely filled with water and hence a formation in the marine-phreatic environment. Microdolomite inclusions and partly mottled CL of RFCs indicate that some diagenetic overprint has occurred whereas zones of nonluminescence represent minimal alteration. CL patterns and the degree of alteration are in good agreement with $MgCO_3$ contents, which is higher in areas of low overprint. Maximum values of 8.5 mole% were obtained from analyses in areas of high microdolomite-inclusion density. Mean $MgCO_3$ contents are even higher than those (0.4–1.0 mole%) of Lower Jurassic crinoid ossicles, which had a primary high-Mg calcite (HMC) composition. Sr concentrations of RFCs correspond well to values of Lower Jurassic crinoids (mean 430 ppm) indicating an HMC precursor that stabilized to LMC and dolomite in a partly closed system. In an open system, Mg would have been dissipated completely and not re-precipitated in situ as microdolomite. Low Mn and Fe concentrations point to oxidizing redox conditions during precipitation. In contrast, zones of strong alteration are characterized by mottled, bright-yellow CL caused by Mn concentrations up to 2,760 ppm. Incorporation of Mn into the calcite lattice, associated with low Fe, concentrations is typical for marine shallow-burial conditions or a deeper, suboxic level of a meteoric–phreatic environment. Diagenetic alteration of RFCs during shallow-burial diagenesis is also reported from the Steinplatte and Wilde Kirche (Mazzullo et al. 1990; Satterley et al. 1994).

Reference values of oxygen-isotope values for Rhaetian seawater were obtained from brachiopods of the Kössen Beds (Korte et al. 2005), which represent a very wide spectrum of palaeo-seawater temperatures (Fig. 9). However, assuming a $\delta^{18}O$ of 0‰ (V-SMOW) for Triassic seawater and applying the equations of O'Neil et al. (1969) and Hays and Grossman (1991), the −0.6 to 1.2‰ range of diagenetically unaltered RFCs would correspond to temperatures of 18–21°C. This seems to be too cold for a tropical marine environment as it is expected for the Adnet reef because such low temperatures are close to the tolerance limit of reef-building corals (Kleypas et al. 1999). Values obtained from the carbonate matrix and IS I of the Adnet reef seem to come nearer to its pristine seawater composition (Fig. 7). Therefore, the heavy oxygen-isotope values of RFCs are probably due to a precipitation in deeper (colder) water in the first phase of drowning of the platform in Mid-Hettangian times. This assumption is also supported by the similarity of stable-isotope values of RFCs with those of the Lower Sinemurian Adnet Formation (Figs. 7, 9). Also, Satterley et al. (1994) interpreted RFCs as marine cements formed *after* drowning in Early Jurassic times. Mazzullo et al. (1990), however, interpreted the RFCs as marine precipitates altered by meteoric pore water during shallow burial. The alternation in the diagenetic succession is explained by Mazzullo et al. (1990) as the effect of high-frequency, small-scale, sea-level changes during the Hettangian *prior* to the final drowning of the platform.

Partly corroded RFC crystal tips overlain by crystal silt indicate dissolution and erosion within cavities, a phenomenon also observed by Mazzullo et al. (1990) and Satterley et al. (1994) at the Steinplatte and Wilde Kirche reef complexes and interpreted as caused by meteoric influx. Renewed meteoric influence, however, is unlikely after drowning of the platform in the Mid-Hettangian to Early Sinemurian when water depth was probably beyond 50 m (Garrison and Fischer 1969; Böhm 1992) (Fig. 3). Böhm et al. (1999) reported a slight sea-level fall in the Late Hettangian, which led to enhanced current activity which in turn caused strong condensation and the formation of the 'Marmorea Crust'. This could have also affected parts of the pore space of the Adnet reef leading to submarine dissolution and erosion.

Dog-tooth cement II

Dog-tooth cement II syntaxially overgrows RFC and marks a major change in crystal habit (Fig. 8d, f). Crystals are clear, scalenohedral in shape, up to 250 μm in length and show irregular growth directions. Microdolomite inclusions are common. Dog-tooth cement II is nonluminescent with a bright-yellow zone on the outer margin of the crystals (Fig. 8d, f). It is composed of LMC with $MgCO_3$ contents of 0.01–2.1 mole%. Sr concentrations are between <200 and 1,660 ppm, Mn and Fe concentrations are mostly below detection limit. In the bright-luminescent outer zones of the crystals, Mn concentration is elevated with values of 1,070–6,260 ppm. As with dog-tooth cement I, crystals are too small to be sampled for stable-isotope analyses.

Nonluminescence and low Fe^{2+} concentrations of dog-tooth cement II indicate precipitation from oxidizing pore water in the marine to shallow-burial environment. In contrast to dog-tooth cement I, microdolomite inclusions indicate an original HMC mineralogy.

The bright-yellow luminescent outer margin of dog-tooth cement II indicates a significantly increased Mn^{2+} concentration in the calcite lattice compared to the previous nonluminescent core. The non/bright CL transition is generally interpreted as a decrease in redox potential (Eh), which results in reduction of Mn^{4+} to Mn^{2+} and leading to solution of Mn^{2+} and incorporation into the calcite lattice. Decreasing Eh is expected under conditions of progressive marine burial (Drever 1982) and is thus also presumed to be responsible for the Mn uptake at the non-to-bright CL transition in dog-tooth cement II. Dog-tooth cements overgrowing RFCs and displaying nonluminescence with bright-luminescent outer margins are well known from several diagenetic studies (e.g. Kerans et al. 1986; Lavoie and Bourque 1993; Kaufmann 1997).

Internal sediment II

Internal sediment II (IS II) sometimes postdates RFCs and IS I in dissolution cavities. It is red to purple in colour, geopetally layered, and consists of micrite which contains coarse skeletal debris, e.g. crinoid ossicles, mollusc remains, ostracods and benthic foraminifers (Fig. 5f). Thus, IS II lithologically strongly resembles the red crinoid-rich biomicrites of the Adnet Formation (Lower Sinemurian). CL of IS II is mottled yellow–orange. Stable-isotope analyses of five samples show mean values of $\delta^{18}O = -0.8$ (±0.4)‰ and $\delta^{13}C = +2.5$ (±0.4)‰ (Fig. 7).

IS II was probably washed into the dissolution cavities during Lower Sinemurian times. This is not only evidenced by the lithological similarity with the Lower Sinemurian Adnet Formation but also by correspondent stable-isotope signatures (Fig. 7). Compared to oxygen-isotope analyses of IS I, values of IS II are significantly heavier and can thus easily be distinguished.

Silifications

Selective, mottled silifications consisting of chalcedony and microquartz occur in 10–15% of the *Retiophyllia* corallites (Fig. 5g) and along crystal boundaries and cleavage surfaces of RFCs. They are whitish to yellowish, unregular-spheroidal, and 2–3 mm in size. Due to sparse occurrence and small size investigations of crystallization and geochemistry were not undertaken.

To the authors state of knowledge, this is the first description of silifications from Rhaetian reefs of the Northern Calcareous Alps. Since siliceous organisms are absent in the Adnet reef and silifications clearly postdate RFCs, a late diagenetic origin is assumed. As a source of SiO_2, transformations of clay minerals (e.g. montmorillonite-illite) during a late stage of burial can be considered.

Blocky calcite cement

Clear, equant, partly ferroan blocky calcite cements fill remaining void space of dissolution cavities (Fig. 8c–f). CL is uniform orange or concentrically zoned bright- and dull-orange parallel to growth direction. The dull-orange luminescent zones reveal elevated Fe contents as also evident by potassium ferricyanide staining. Microprobe analyses yielded Sr concentrations of below detection limit to 630 ppm and Mn and Fe concentrations of below detection limit to 5,850 and 840 ppm, respectively. Five stable-isotope analyses of blocky calcites display mean values of $\delta^{18}O = -5.7$ (±1.1)‰ and $\delta^{13}C = +2.8$ (±0.1)‰ (Fig. 9).

The partly ferroan, blocky calcite cements are certainly of burial origin. The increased Fe content is usually considered as the result of more reducing redox conditions with Fe^{2+} in solution derived from clay minerals. Fluctuating redox conditions in the marine-derived pore water are most probably the origin of the alternating CL pattern. Average $\delta^{18}O$ values are 4.4‰ lighter than those of RFCs (Fig. 9), whereas the $\delta^{13}C$ values are slightly higher (+0.4‰). Excluding an input of exotic fluids and diagenetic alteration and assuming temperature as the primary control for the $\delta^{18}O$ values of blocky calcite cements, precipitation temperature and burial depth can be estimated (e.g. Hurley and Lohmann 1989; Lavoie and Bourque 1993). According to Friedman and O'Neil (1977), each 10°C increase in temperature causes a negative $\delta^{18}O$ shift of ca. 2.0‰. The observed shift of −2.5 to −5.2‰ thus corresponds to an increase in pore-water temperature of 12.5–26°C with respect to

the RFCs that precipitated under marine-phreatic conditions. Assuming a normal geothermal gradient of 30°/km in the Adnet area, 420–870 m of burial is required to accommodate the oxygen-isotope values of the blocky calcite cements. However, these values are only a rough estimate, because the isotopic evolution of porewaters is influenced by many other factors in addition to temperature (e.g. salinity and others). If the above burial estimates are correct, then precipitation of the blocky calcite cements would have occurred in the Early Cretaceous (Garrison and Fischer 1969; Kramer and Kröll 1979; Plöchinger 1990). Interestingly, the $\delta^{13}C$ values show no depletion with respect to RFCs. Typically, thermocatalytic decarboxylation of organic matter occurs in burial depths of several hundred meters (Irwin et al. 1977) releasing ^{12}C-enriched CO_2 into pore waters thus causing a depletion of $\delta^{13}C$ values in late blocky calcite cements (e.g. Hurley and Lohmann 1989; Kaufmann 1997).

Blocky calcite cements of the Wilde Kirche reef complex with comparable CL patterns and stable-isotope composition were interpreted by Satterley et al. (1994) as shallow-burial in origin. These authors assumed an elevated geothermal gradient related to peak rifting activity of the Tethyan margins in the Middle to Late Jurassic. In contrast, blocky calcite cements of coeval reef limestones of the Steinplatte complex with similar oxygen-isotope values but low Mn concentrations are suggested as meteoric in origin formed prior to terminal burial in the Sinemurian (Mazzullo et al. 1990).

Saddle dolomite

Saddle dolomite is the youngest phase in the diagenetic sequence of the Adnet reef. It locally replaces blocky calcite cement or fills remaining pore space. Crystals are sub- to euhedral, 200–300 μm in size and display the typical curved crystal and cleavage surfaces with stepped offsets and undulose extinction.

Saddle dolomite is usually interpreted to be the product of hydrothermal-hypersaline pore water and deep-burial diagenesis. Precipitation temperatures are assumed to be higher than 60°C (Radke and Mathis 1980; Gregg 1983). Assuming a normal geothermal gradient (30°C/km), such high temperatures could hardly have been reached in the Adnet reef at maximum burial depths of ca. 1,000 m (Plöchinger 1990). Therefore, an elevated heat flow or hydrothermal influences related to compressional subduction regimes of the Penninic Ocean are the most probable cause of such hot brines. Saddle dolomite as latest diagenetic phase is also documented from the Wilde Kirche reef complex (Satterley et al. 1994).

Neptunian dikes

In the Lienbacher Bruch (Fig. 1c), the 'Marmorea Crust' unconformably separates the Rhaetian reef limestone (bioclastic grainstones with isolated *Retiophyllia* colonies) from the overlying red, crinoid-rich biomicrites of the Lower Sinemurian Adnet Formation. The latter are also found in neptunian dikes of the Tropfbruch quarry. The boundary between dike and host rock is mostly straight, rarely irregular with the red filling penetrating a few centimeters into the red bioclastic grainstones of the Rhaetian reef limestone. Isolated corallites are cut by the dikes; in a few cases, the RFCs within dissolved corallites are deeply eroded and the resulting cavity is filled with laminated crystal silt and red biomicrite. Hence, RFCs in neptunian dikes must be older than Early Sinemurian, the age of the basal Adnet Formation. Frequently, the surface of the neptunian dikes is covered by a narrow, isopachous seam of 100 μm-sized bladed to rarely dog-tooth-like calcite cements, overgrowing both corallites and sediment. Individual crystals have irregular crystal tips suggesting corrosion. The calcite cement crust is separated from the red infill of the dike by a thin ferromanganese crust. At a few places, the surface of one dike examined shows evidence of tectonic movement. Along the surface, a 5-mm-wide set of joints is developed that contains deformed and curved fibrous calcites. This points to a displacement of crystals during the movement.

The neptunian dikes are interpreted as having formed by synsedimentary faulting in the Mid-Hettangian. The presence of deformed fibrous calcites also indicates tectonic activity in this interval. Marine bladed or fibrous calcites precipitated show corrosion before a ferromanganese crust (probably corresponding to the Upper Hettangian 'Marmorea Crust') was formed and deeper marine red biomicrites of the Adnet Formation were deposited in the dike. In the present study, corrosion of fibrous calcites followed by sedimentation of crystal silt is interpreted, corresponding to the corrosion of RFCs in dissolution cavities, by submarine dissolution, and erosion. These could have been caused by enhanced bottom currents during sea-level lowstand in the Late Hettangian (Böhm et al. 1999).

Development of the diagenetic sequence of the Adnet reef and its control by sea-level changes

The overall diagenetic evolution of the Adnet reef can be divided into subsequent stages that are controlled by sea-level changes and the sedimentary evolution at the margin of the Dachstein carbonate platform (Fig. 10). Changes between marine and meteoric diagenesis are probably caused by sea-level fluctuations.

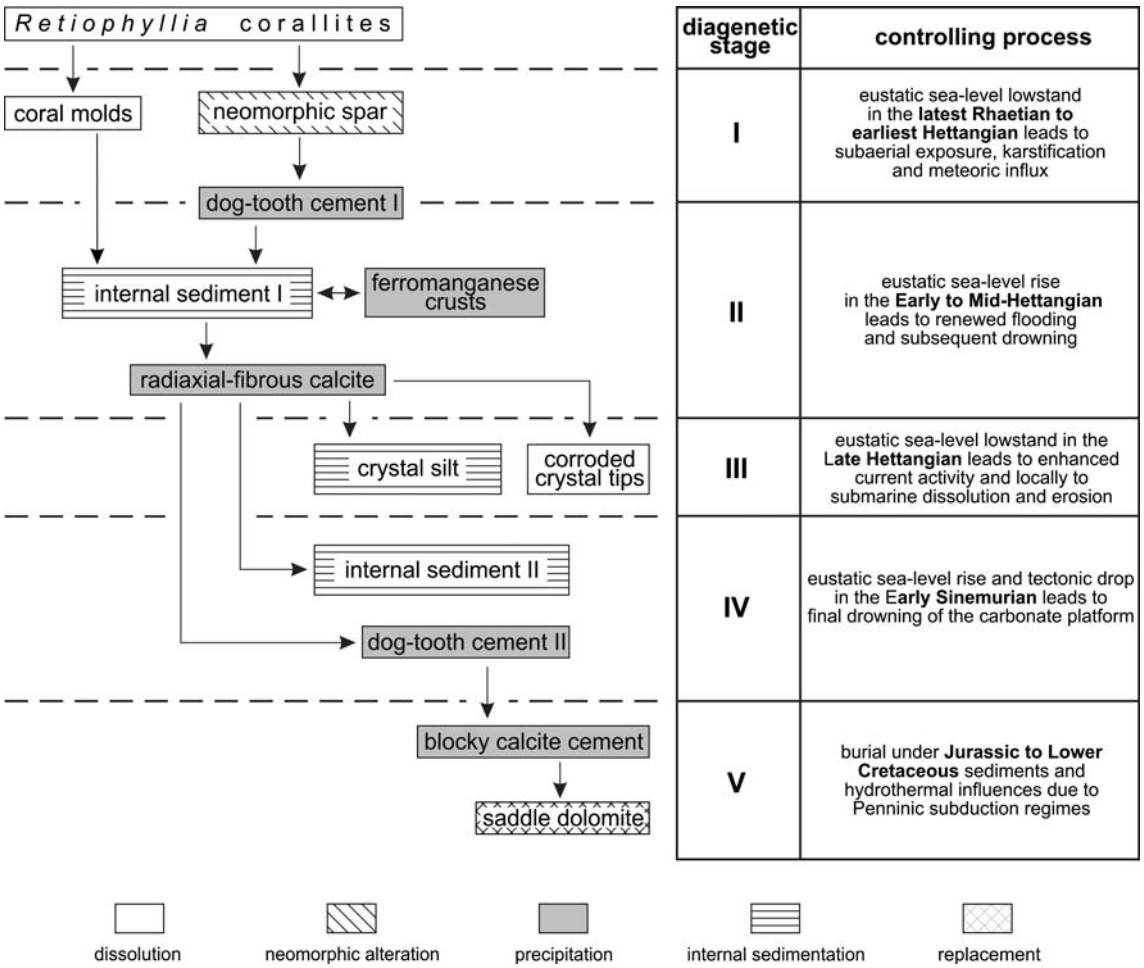

Fig. 10 Sequence of diagenetic products in *Retiophyllia* corallites in relation to subsequent diagenetic stages

The global eustatic sea-level curve (Haq et al. 1988; Hallam 1988) shows a distinct regression at the Triassic–Jurassic boundary. In the Early to Mid-Hettangian, a renewed transgression and highstand phase occurred passing into a regression at the end of the stage. At the Hettangian–Sinemurian boundary, a renewed transgression is observed. These eustatic sea-level curves, however, do not take into account high-frequent, small-scale eustatic sea-level changes and regional tectonics. Nevertheless, the latter are deciding factors in the development of the sedimentary succession at the Triassic–Jurassic transition of the Northern Calcareous Alps.

Stage I (latest Rhaetian to earliest Hettangian): eustatic sea-level falls resulting in subaerial exposure, karstification, meteoric dissolution, and cementation

A eustatic sea-level fall shortly before to the Triassic–Jurassic boundary caused subaerial exposure of the Adnet reef. The karstification of the reef surface and the meteoric dissolution of aragonitic coral skeletons and sediment is expressed in the formation of dissolution cavities. Coral septa that escaped dissolution were transformed into *neomorphic calcite spar* by meteoric pore water. Later, *dog-tooth cement I* of LMC mineralogy precipitated sporadically on the altered coral skeletons.

The amplitude of sea-level fall immediately prior to the Triassic–Jurassic boundary was too small to leave traces in the continuous sedimentary succession of the adjacent basin (Böhm et al. 1999; Kuerschner et al. 2007) and is assumed to be in the order of 10–20 m. This assumption is supported by the fact that the depth of karstification below the Triassic–Jurassic unconformity is only 2 m (Bernecker et al. 1999) and hence the reef core was hardly uplifted above sea level. From the Adnet reef, Bernecker et al. (1999) reported two previous intra-Rhaetian phases of emergence (Fig. 2, 3).

Subaerial exposure and karstification at the Triassic–Jurassic boundary are widespread in the Northern Calcareous Alps (Stanton and Flügel 1989; Mazzullo et al. 1990; Satterley et al. 1994). Satterley et al. (1994) reported an emergence of 5–15 m of the Wilde Kirche reef complex

and assumed a duration of subaerial exposure of 10–50 ka. This short interval is suggested by the small size of dissolution cavities (10 cm on average), which indicates a rather short influence of meteoric waters (White 1984; Smart and Whitaker 1991). Mazzullo et al. (1990), however, assume a much longer period of emergence of the Steinplatte complex comprising the latest Rhaetian to Early Hettangian, approximately 1.0 Ma (Fig. 3).

The outcrop situation of the Adnet quarries allows a clear separation of the timing of (1) the three levels of karstification in the latest Rhaetian, and (2) synsedimentary faulting in the Early Jurassic. Nowhere in the outcrop were synsedimentary faults found to have originated already in Triassic times because neptunian dikes are always filled with red Jurassic sediments but never with uppermost Rhaetian reefal sediments (see also 'Neptunian dikes'). Therefore, subaerial exposure and karstification in the Adnet reef were probably related to small-scale eustatic sea-level falls in the latest Rhaetian, when progradation and expansion of the platforms were accelerated due to a global eustatic sea-level lowstand (Haq et al. 1988; Hallam 1988).

Stage II (Early- to Mid-Hettangian): eustatic sea-level rise caused reflooding, internal sedimentation, and cementation

Eustatic sea-level rise following subaerial exposure at the Triassic–Jurassic boundary caused reflooding and subsequent drowning of the Adnet reef during Hettangian times. Drowning is enhanced by tectonic activity as evidenced from the opening of neptunian dikes. Sediments of the Hettangian Schnöll Formation progressively onlapped onto the reef slope (Böhm et al. 1999; Krystyn et al. 2005) whereas the reef core remained uncovered due to its steep relief and submarine erosion by bottom currents. Pore spaces of the Adnet reef, however, were refilled by marine water and *internal sediments* (IS I), derived from the karstified host rock of the Upper Rhaetian reef limestone, are washed in.

Radiaxial-fibrous calcites of HMC composition normally postdate IS I and were precipitated in deeper (=colder) water in the first phase of drowning in Mid-Hettangian times as shown by their heavy oxygen-isotope values.

Stage III (Late Hettangian): eustatic sea-level lowstand causing submarine dissolution and erosion

In the Late Hettangian, a ferromanganese crust ('Marmorea Crust') is developed on the drowned Adnet reef separating it from the overlying Lower Sinemurian Adnet Formation (Böhm et al. 1999). This crust is also present in neptunian dikes and even in basinal settings and is thus certainly related to an overall phase of omission due to an intermediate phase of eustatic sea-level lowstand at this time (Haq et al. 1988; Hallam 1988). Böhm et al. (1999) interpreted the 'Marmorea Crust' as the result of increased bottom currents leading to erosion and/or omission. The enhanced current activity probably also partly affected the Adnet reef's pore space as shown by submarine dissolution and erosion (corroded crystal tips of RFCs and sedimentation of crystal silt).

Stage IV (Early Sinemurian): tectonic drops and eustatic sea-level rise causing final, rapid drowning, and renewed internal sedimentation and cementation

In the Early Sinemurian, the combination of tectonic drop and eustatic sea-level rise (Haq et al. 1988; Hallam 1988) resulted in rapid drowning of the Dachstein carbonate platform. Significant tectonic activity at this time is probably related to rotational block faulting on the southern continental margin of the Tethys (Lackschewitz et al. 1991). Deposition of the Adnet Formation levels the Adnet reef's relief and sediments also intrude dissolution cavities forming a second generation of red *internal sediments* (IS II). Where these internal sediments are absent, RFCs are syntaxially overgrown by *dog-tooth cement II* indicating a change in crystal habit and, with its bright-luminescent outer margin, a transition to reducing redox conditions in the pore water during progressive burial.

Stage V (Early Cretaceous): burial diagenesis and hydrothermal influences

Occlusion of the remaining pore space with blocky calcite cements occurred under elevated temperatures of ca. 30–50°C at burial depths of 420–870 m as shown by their depleted oxygen-isotope values. Thus, based on stratigraphic reconstruction, precipitation of blocky calcite cements must have occurred in the Early Cretaceous. Fe incorporation is due to strongly reducing redox conditions with Fe^{2+} in the pore water leached from clay minerals.

Formation of saddle dolomite as latest diagenetic phase in the Adnet reef is probably due to hydrothermal influences related to compressional subduction regimes of the Penninic Ocean.

Acknowledgments Johannes H. Schroeder (Berlin) initiated this study, acted as supervisor, and has raised funds from the Deutsche Forschungsgemeinschaft (DFG) (project Schr 257/4-1). The project was performed within the scope of the DFG priority program "Globale und regionale Steuerungsprozesse biogener Sedimentation, Themenkreis 1: Riff Evolution". Technical help (thin sections) was provided by Kerstin Döbbern, Markus Stöwer, Constanze von Engelhardt, Silke Becker (all Technische Universität, Berlin) and Franz Tscherne (Graz). Francois Galbert assisted during microprobe analyses. Anselm Loges (Tübingen) helped during cathodoluminescence microscopy. Stable isotopes were analyzed by Michael

M. Joachimski (Erlangen). Erik Flügel (deceased), Michaela Bernecker (Muscat, Oman), Oliver Weidlich (Wintershall, Kassel) and Heinrich Zankl (Marburg) are acknowledged for joint field works and discussions. Jobst Wendt (Tübingen) read an earlier draft of the manuscript and provided many corrections. Finally, journal reviewers Rüdiger Henrich (Bremen) and János Haas (Budapest) enormously improved the paper by contributing their experience in the geology of the Northern Calcareous Alps.

References

Bernecker M, Weidlich O, Flügel E (1999) Response of Triassic reef coral communities to sea-level fluctuations, storms and sedimentation: evidence from a spectacular outcrop (Adnet, Austria). Facies 40:229–280

Böhm F (1992) Mikrofazies und Ablagerungsmilieu des Lias und Dogger der Nordöstlichen Kalkalpen. Erl Geol Abh 121:57–217

Böhm F, Ebli O, Krystyn L, Lobitzer H, Rakús M, Siblík M (1999) Fauna, Biostratigraphie und Sedimentologie des Hettang und Sinemur (Unterlias) von Adnet, Salzburg, Österreich). Abh Geol Bundesanst 56:143–271

Drever JI (1982) The geochemistry of natural waters. Prentice Hall, New Jersey, p 288

Fischer AG (1964) The Lofer cyclothems of the Alpine Triassic. In: Merriam DF (ed) Symposium on cyclic sedimentation. Kansas Geol Surv Bull 169:107–149

Flügel E, Koch R (1995) Controls on the diagenesis of Upper Triassic carbonate ramp sediments: Steinplatte, Northern Alps (Austria). Geol Paläont Mitt Innsbruck 20:283–311

Flügel E, Tietz G-F (1971) Über die Ursachen der Buntfärbung in Oberrhät-Riffkalken (Adnet, Salzburg). N Jb Geol Paläont Abh 139:29–42

Friedman I, O'Neil JR (1977) Compilation of stable isotope fractionation factors of geochemical interest. In: Fleischer M (ed) Data of geochemistry (6th edn), US Geol Surv, Prof Pap 440(K):1–12

Garrison RE, Fischer AG (1969) Deep water limestones and radiolarites of the Alpine Jurassic. In: Friedman GM (ed) Depositional environments of carbonate rocks. SEPM Spec Publ 14:20–56

Given RK, Wilkinson BH (1985) Kinetic control of morphology, composition, and mineralogy of abiotic sedimentary carbonates. J Sed Petrol 55:109–119

Gregg JM (1983) On the formation and occurrence of saddle dolomite–discussion. J Sed Petrol 53:1025–1033

Haas J (1991) A basic model for Lofer cycles. In: Einsele G, Ricken W, Seilacher A (eds) Cycles and events in stratigraphy. Springer, Berlin, pp 722–732

Hallam A (1988) A reevaluation of Jurassic eustasy in the light of new data and the revised Exxon curve. In: Wilgus CK, Hastings BS, Kendall CGStC, Posamentier HW, Ross CA, Van Wagoner JC (eds) Sea-level changes: an integrated approach. SEPM Spec Publ 42:261–273

Haq BU, Hardenbol J, Vail PR (1988) Mesozoic and Cenozoic chronostratigraphy and cycles of sea-level change. In: Wilgus CK, Hastings BS, Kendall CGStC, Posamentier HW, Ross CA, Van Wagoner JC (eds) Sea-level changes: an integrated approach. SEPM Spec Publ 42:71–108

Hays PD, Grossman EL (1991) Oxygen isotopes in meteoric calcite cements as indicators of continental paleoclimate. Geol 19:441–444

Hurley NF, Lohmann KC (1989) Diagenesis of Devonian reefal carbonates in the Oscar Range, Canning Basin, Western Australia. J Sed Petrol 59:127–146

Irwin H, Curtis CD, Coleman M (1977) Isotopic evidence for source of diagenetic carbonates formed during burial of organic-rich sediments. Nature 269:209–213

Kaufmann B (1997) Diagenesis of Middle Devonian carbonate mounds of the Mader Basin (eastern Anti-Atlas, Morocco). J Sed Res A67:945–956

Kerans C, Hurley NF, Playford PE (1986) Marine diagenesis in Devonian reef complexes of the Canning Basin, Western Australia. In: Schroeder JH, Purser BH (eds) Reef diagenesis. Springer, Berlin, pp 358–380

Kleypas JA, McManus JW, Meñez LAB (1999) Environmental limits to coral reef development: where do we draw the line? Am Zool 39:146–159

Korte C, Kozur HW, Veizer J (2005) δ^{13}C and δ^{18}O values of Triassic brachiopods and carbonate rocks as proxies for coeval seawater and palaeotemperature. Palaeogeogr Palaeoclimatol Palaeoecol 226:287–306

Kramer H, Kröll A (1979) Die Untersuchungsbohrung Vigaun U 1 bei Hallein in den Salzburger Kalkalpen. Mitt österreich geol Ges 70:1–10

Krystyn L, Böhm F, Kürschner W, Delecat S (2005) The Triassic–Jurassic boundary in the Northern Calcareous Alps. 5th Field Workshop IGCP 458 Project, A:1–39

Kuerschner WM, Nina R, Bonis NR, Krystyn L (2007) Carbon-isotope stratigraphy and palynostratigraphy of the Triassic–Jurassic transition in the Tiefengraben section: Northern Calcareous Alps (Austria). Palaeogeogr Palaeoclimatol Palaeoecol 244:257–280

Lackschewitz KS, Grützmacher U, Henrich R (1991) Paleoceanography and rotational block faulting in the Jurassic carbonate series of the Chiemgau Alps (Bavaria). Facies 24:1–24

Lavoie D, Bourque P-A (1993) Marine, burial, and meteoric diagenesis of Early Silurian carbonate ramps, Quebec Appalachians. Can J Sed Petrol 63:233–247

Mandl GW (2000) The Alpine sector of the Tethyan shelf: examples of Triassic to Jurassic sedimentation and deformation from the Northern Calcareous Alps. Mitt Österreich Geol Ges 92:61–77

Marcoux J, Baud A, Ricou L-E, Gaetani M, Krystyn L, Bellion Y, Guiraud R, Besse J, Gallet Y, Jaillard E, Moreau C, Theveniaut H (1993) Late Norian (215–212 Ma). In: Dercourt J, Ricou LE, Vrielynck B (eds) Atlas Tethys palaeoenvironmetal maps, explanatory notes. Gauthier-Villars, Paris, pp 35–53

Mazzullo SJ, Bischoff WD, Lobitzer H (1990) Diagenesis of radiaxial fibrous calcites in a subunconformity, shallow-burial setting: Upper Triassic and Liassic, Northern Calcareous Alps, Austria. Sedimentology 37:407–425

Mirsal IA, Zankl H (1979) Petrography and geochemistry of carbonate void-filling cements in fossil reefs. Geol Rundsch 68:920–951

O'Neil JR, Clayton RN, Mayeda TK (1969) Oxygen isotope fractionation in divalent metal carbonates. J Chem Phys 51:5547–5558

Pálfy J (2008) The quest for refined calibration of the Jurassic time-scale. Proc Geol Assoc 119:85–95

Piller WE (1981) The Steinplatte reef complex, part of an Upper Triassic carbonate platform near Salzburg, Austria. In: Toomey DF (ed) European fossil reef models. SEPM Spec Publ 30:261–290

Plöchinger B (1990) Geologische Karte der Republik Österreich. Erläuterungen zu Blatt 94 Hallein. Geol Bundesanst, pp 1–79

Radke RM, Mathis RL (1980) On the formation of saddle dolomite. J Sed Petrol 50:1149–1168

Reinhold C (1999) Dog-tooth cements: indicators of different diagenetic environments. Zbl Geol Paläont Teil I 1997:1221–1235

Stanton RJ Jr, Flügel E (1989) Problems with reefs models: the late Triassic Steinplatte "reef" (Northern Alps, Salzburg/Tyrol, Austria). Facies 20:1–138

Satterley AK, Marshall JD, Fairchild IJ (1994) Diagenesis of an Upper Triassic reef complex, Wilde Kirche, Northern Calcareous Alps, Austria. Sedimentology 41:935–950

Schäfer P (1979) Fazielle Entwicklung und palökologische Zonierung zweier obertriadischer Riffstrukturen in den nördlichen Kalkalpen (Oberrhät-Riff-Kalke, Salzburg). Facies 1:3–245

Smart PL, Whitaker FF (1991) Karst processes, hydrology, and porosity evolution. In: Wright VP (ed) Palaeokarsts and palaeokarstic reservoirs. Postgrad Res Inst Sed Occ Publ Ser 2, pp1–55

White WP (1984) Rate processes: chemical kinetics and karst landform development. In: La Fleur RG (ed) Groundwater as a geomorphic agent. Oxford University Press, Oxford, pp 227–248

Wurm D (1982) Mikrofazies, Paläontologie und Palökologie der Dachsteinriffkalke (Nor) des Gosaukammes, Österreich. Facies 6:203–296

Zankl H (1969) Der Hohe Göll. Aufbau und Lebensbild eines Dachsteinkalk-Riffes in den Nördlichen Kalkalpen. Abh Senckenberg Naturforsch Ges 519:1–123

Zankl H (1971) Upper Triassic carbonate facies in the Northern Limestone Alps. In: Müller G (ed) Sedimentology of parts of Central Europe, Guidebook VIII. Int Sed Congr, pp 147–185